Spontaneous Aqueous Defluorination of Trifluoromethylphenols: Substituent Effects and Revisiting the Mechanism

Zhefei Guo[1‡], Geneviève W. Tremblay[1‡], Jingdan Chen[2], Shira Joudan[1*]

[‡]Z.G. and G.W.T. contributed equally to this work

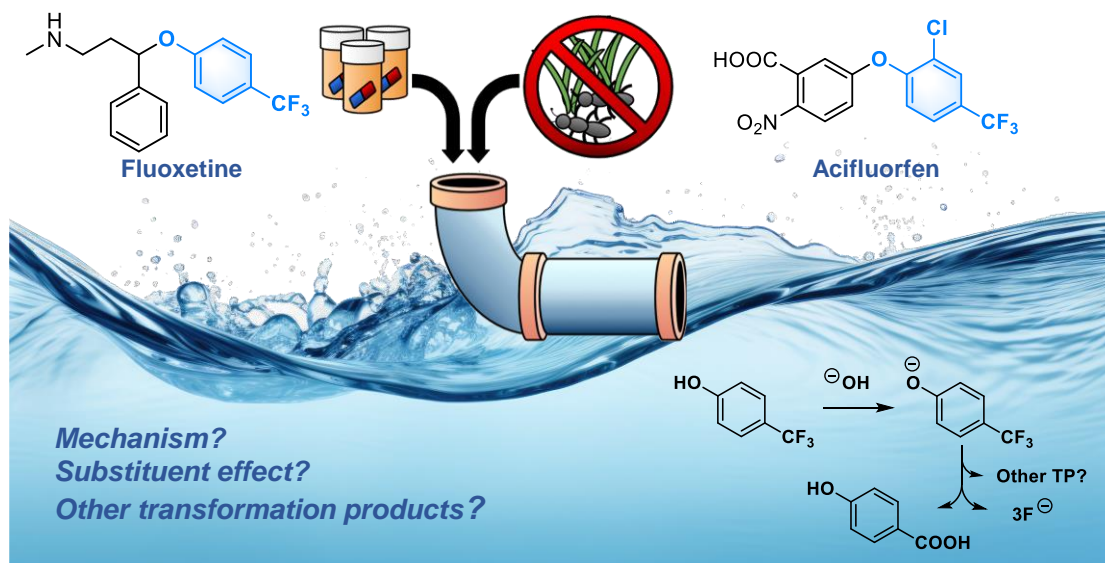[1]Department of Chemistry, University of Alberta, Edmonton T6G 2G2, Alberta, Canada

[2]Department of Chemistry, University of Illinois at Urbana-Champaign, Urbana, Illinois 61801, United States

Email: joudan@ualberta.ca

12 TOC/Abstract Art

Fluoxetine

Acifluorfen

Mechanism?
Substituent effect?
Other transformation products?

Other TP?

3F

14 Environmental Significance

15 The environmental transformation of some aryl-CF_3 pharmaceuticals and agrochemicals

16 produces trifluoromethylphenols (TFMPs), which are environmental contaminants themselves

17 and can be precursors to the very persistent pollutant trifluoroacetic acid (TFA). Alternatively,

18 this study demonstrates that certain TFMPs can undergo complete hydrolytic defluorination in

19 aqueous solutions, depending on their chemical structure. Understanding what drives this

20 spontaneous defluorination can provide insight into why certain C−F bonds can break, despite

21 the general stability of organofluorine compounds. Designing aryl-CF_3 compounds to favor

22 defluorination pathways without TFA formation could harness the benefits of the –CF_3 moiety

23 in pharmaceuticals and agrochemicals while reducing their environmental persistence.

ABSTRACT

Trifluoromethylphenols (TFMPs) are environmental contaminants that exist as transformation products of aryl-CF$_3$ pharmaceuticals and agrochemicals. Their −CF$_3$ moiety raises concerns as it may form problematic fluorinated transformation products such as the persistent pollutant trifluoroacetic acid (TFA). This study investigates the hydrolysis and spontaneous defluorination mechanisms of 2-TFMP, 3-TFMP, 4-TFMP, and 2-Cl-4-TFMP under environmentally relevant aqueous conditions, and under alkaline pH to investigate the mechanism of defluorination. 3-TFMP did not undergo hydrolysis. The other TFMPs reacted to primarily form the corresponding hydroxybenzoic acids and fluoride. High-resolution mass spectrometry identified a benzoyl fluoride intermediate in the hydrolysis of 4-TFMP and other dimer-like transformation products of the 4- and 2-Cl-4-TFMP. Density functional theory calculations revealed that the key defluorination step proceeds via an E1cb mechanism, driven by β-elimination. Experimental and computational results demonstrated substituent-dependent differences in reactivity, and the importance of the deprotonation of TFMPs for the hydrolysis reaction to proceed. These findings provide mechanistic insights into the complete defluorination of TFMPs and broader implications for the environmental defluorination of other PFAS.

INTRODUCTION

Trifluoromethylphenols (TFMPs) are important building blocks for many pharmaceuticals and agrochemicals containing aromatic trifluoromethyl (aryl-CF$_3$) functional groups (**Figure 1A**).[1,2] Fluorine (F) has a small atomic radius, the highest electronegativity, and forms strong bonds with carbon.[3] By substituting all hydrogens in a methyl group (−CH$_3$) with F atoms, the performance of aryl-CF$_3$ products are often enhanced through, for example, increased metabolic stability and lipophilicity.[3] However, the high stability of C−F bonds raises concerns about the persistence of these compounds and their fluorinated transformation products (TPs) in the environment.[4,5] For example, the well-recognized TP of fluoxetine 4-(trifluoromethyl)phenol (4-TFMP)[6–8] produces the very persistent and very mobile pollutant trifluoroacetic acid (TFA) via photochemical reactions.[7,9,10] 2-Cl-4-TFMP is a TP of diphenyl ether herbicides like acifluorfen, oxyfluorfen and fluoroglycofen,[11–13] yet its environmental chemistry has not been studied. In addition to their identification as transformation products in laboratory studies, 3-TFMP and 4-TFMP have been measured in the environment.[14,15] Aryl-CF$_3$ compounds are classified as per- and polyfluoroalkyl substances (PFAS) according to OECD definition,[16,17] and therefore are receiving heightened interest. Understanding the environmental reactivity of TFMPs is essential for understanding the environmental fate of many aryl-CF$_3$ pharmaceuticals and agrochemicals.

Hydrolysis is an important abiotic transformation pathway for organic pollutants. Previous research observed that 2- and 4-TFMP can undergo hydrolysis resulting in spontaneous defluorination under alkaline conditions.[6,9,18–23] Reuben G. Jones first reported the base-mediated defluorination of 4-TFMP in 1947, observing that higher concentrations of 4-TFMP

65 spontaneously defluorinated and polymerized in NaOH solutions, eventually stabilizing with

66 no further defluorination.[18] Later, in 1973, Sakai and Santi observed complete hydrolytic

67 defluorination of 2- and 4-TFMP in buffered solutions (pH 6.5 – 13), yielding 2- and 4-

68 hydroxybenzoic acid (2- and 4-HBA), respectively.[19] More recently, environmental chemists,

69 including the Mabury group,[6,20,21] Manfrin et al.,[22] and Bhat et al.,[9] reported similar

70 defluorination reactions. The spontaneous defluorination of certain TFMPs under

71 environmentally relevant conditions contradicts the common perception that C–F bonds are

72 difficult to activate and that fluoride (F$^-$) is a poor leaving group.[24] The mechanism of this

73 spontaneous defluorination remains largely unexplored due to the lack of identified

74 intermediates (IM) and TPs. No plausible mechanism has been proposed to explain the

75 reactivity differences caused by substituent effects.

76 Density functional theory (DFT) calculations are used in environmental chemistry to

77 calculate the thermodynamics and kinetics of reactions, particularly for environmental

78 chemistry reactions involving reactive transient intermediates that cannot be characterized by

79 common analytical methods.[25–27] By optimizing reactants, intermediates, products, transition

80 states (TS) and calculating the proposed reaction pathways, it is possible to assess the

81 plausibility of these pathways from both thermodynamic and kinetic perspectives. Combined

82 with experimental data, DFT calculations have been successfully applied to explain the

83 degradation of PFAS[25–27] and the hydrolytic defluorination of fluorinated pharmaceuticals.[28]

84
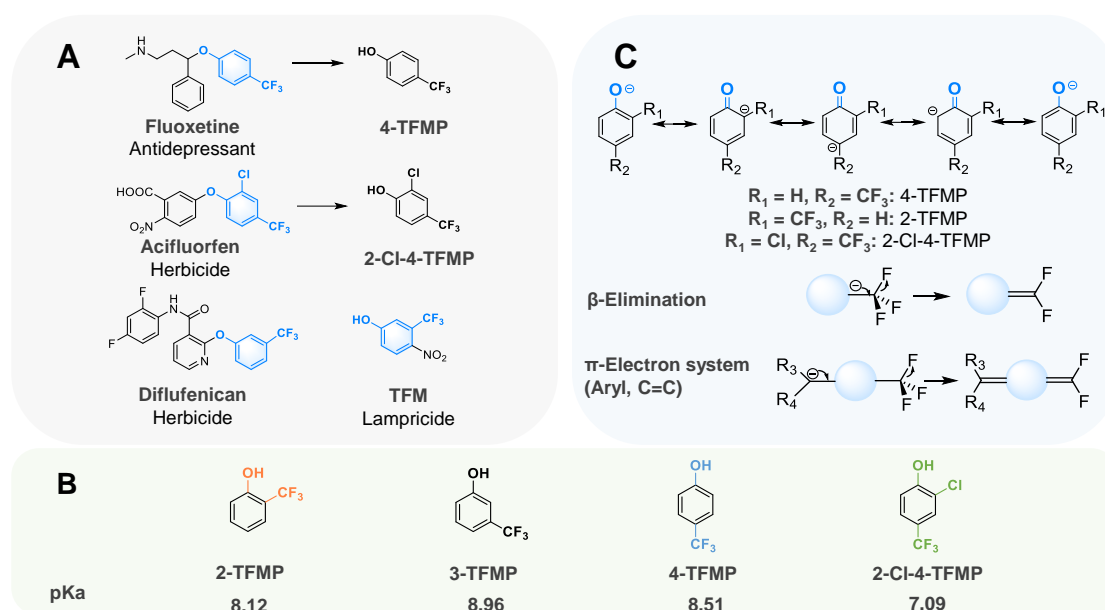
Figure 1. (A) Representative structures of aryl-CF$_3$ pharmaceuticals and agrochemicals containing TFMP building blocks, and reported transformation from aryl-CF$_3$ to TFMPs; (B) TFMP structures studied in this work and their corresponding pKa values; (C) Above, a scheme showing that −CF$_3$ at the *ortho* or *para* position relative to phenol-OH can stabilize the phenolate; below, a reaction scheme showing that β-carbanion drives the defluorination reaction of −CF$_3$.

This study investigated the mechanism of TFMPs that undergo spontaneous defluorination in aqueous solutions under environmentally relevant conditions. To explore the substituent effects, 2-, 3-, 4-, and 2-Cl-4-TFMP were studied in aqueous solutions (**Figure 1B**). Two different pH buffer solutions were used to study the effect of deprotonation on hydrolysis kinetics, and Orbitrap high-resolution mass spectrometry (HRMS) was used to identify TPs. The most plausible spontaneous defluorination mechanism was derived through DFT calculations combined with experimental data.

MATERIALS AND METHODS

Chemicals

All chemicals were used as received and are described in the Supporting Information (**SI-1**).

Hydrolysis Experiments and Analysis

Solutions of 10 mM phosphate (pH 7) or carbonate (pH 10) buffers were prepared in ultrapure water. Stock solutions of 2-, 3-, 4-TFMP (5 mM) and 2-Cl-4-TFMP (1 mM) were prepared in ultrapure water from neat material. Aqueous stock solutions were stored in the dark at 4 °C, and then warmed to room temperature before use. Reaction mixtures were prepared by diluting TFMPs to 10 μM in 10 mM buffers in 100 mL polypropylene volumetric flasks. Experiments were performed in triplicate in polypropylene Falcon tubes wrapped in aluminum foil to minimize exposure to ambient light. Room temperature experiments (~21 °C) were run in a dark drawer with temperatures monitored using an electronic thermometer. To determine the free energy of activation, experiments at pH 10 were also performed at higher temperatures (30 °C and 40 °C) in a hot water bath, where temperatures were recorded with a mercury thermometer. At set time points for each experiment, 1 mL aliquots were mixed with 1M HCl to quench hydrolysis prior to analysis. 5 μL of 1 M HCl was added to the pH 7 aliquots, and 15 μL of 1 M HCl was added to the pH 10 aliquots. The concentrations of TFMPs and their corresponding TPs hydroxybenzoic acids (HBAs) were monitored by high performance liquid chromatography (HPLC) coupled with a UV detector. Detailed instrumental conditions are provided in the **Table S1**. All calibration standards were prepared from neat material dissolved in HPLC grade methanol.

Plotting ln (C_t/C_0) versus time (t) provided the pseudo-first-order rate constants, k (**eq 1**).

The half-lives ($t_{1/2}$) of the compounds were determined from **eq 2**. The Eyring equation (**eq 3**) was used to plot ln (k/T) with respect to $1/RT$ for each experiment (**eq 4**), where k is the pseudo-first order rate constant (s^{-1}); T is the absolute temperature in K; R (8.314 J/(mol·K)) is the gas constant; k_B (1.38 × 10^{-23} J/K) is the Boltzmann constant; h (6.626 × 10^{-34} J·s) is Planck's constant; κ is the transmission coefficient (close to 1 in most cases). The slope of the **eq 4** fitting plot provided the experimental free energy of activation ($\Delta G^{\ddagger}$, kcal/mol).

$$ln\left(\frac{C_t}{C_0}\right) = -kt \qquad \textbf{eq 1}$$

$$t_{1/2} = \frac{0.693}{k} \qquad \textbf{eq 2}$$

$$k = \kappa \frac{k_B T}{h} e^{-\frac{\Delta G^{\ddagger}}{RT}} \qquad \textbf{eq 3}$$

$$ln\frac{k}{T} = -\frac{\Delta G^{\ddagger}}{RT} + ln\frac{k_B}{h} \qquad \textbf{eq 4}$$

To determine the fluorine mass balance of pH 10 hydrolysis experiments, F$^-$ formation was tracked by the Fisherbrand Accumet AB250 pH/ISE meter and fluoride ion selective electrode (ISE). Fluorine mass balance experiments were run in duplicates, and 1 mL aliquots were combined with 1 mL of TISAB II prior to analysis. F$^-$ calibration standards were prepared from NaF dissolved in ultrapure water. TFMPs were also quantified by HPLC-UV in these separate experiments.

The aliquots taken at the beginning and the end of pH 10 hydrolysis experiments were analyzed by ultra-high performance liquid chromatography (UHPLC) coupled with an Orbitrap HRMS to identify TPs. To determine how pH may affect TP formation (i.e., ester formation relying on the deprotonation state of phenol-OH), for 4-TFMP, additional aliquots from pH 7 were also analyzed. Detailed UHPLC-Orbitrap-HRMS parameters are listed in the **Table S2**. Suspected TPs are listed in **Table S6**.

Computational Methods

DFT calculations were performed by the Gaussian 16 (Revision C.01)[29] at 298.15 K and 1 atm. Geometry optimization was calculated at M06-2X/6-311+g(d,p) level of theory. Integral equation formalism polarizable continuum model (IEFPCM) was used to account for solvation effects to structure optimization.[30] Frequency analysis was performed to verify there were no imaginary frequencies for local minima and only one single imaginary frequency for transition states (TS). Single-point energy was calculated at M06-2X/6-311++g(2d,2p) level of theory, as the M06-2X functional is suitable for calculating main group element energies,[31,32] and the same level of theory has been applied to explain the oxidative degradation of PFAS.[25,26]

We specifically considered a hybrid solvation model for key elementary reactions to account for solvation with water. For the explicit solvation, one, two, five, or six explicit H_2O molecules were added to calculations. For the implicit solvation, the solvation free energy was taken into account in the Gibbs free energy (G_f) of a molecule by using solvation model density (SMD) model[33] as indicated by Chen et al.[28] and Qin et al.[34] G_f values were also corrected for the standard state in solution as indicated by Zhang et al.[25,26] For reactions with explicit H_2O molecules, the G_f of H_2O was corrected for its concentration (55.3 M) deviation from its standard state (1 M).[28] Refer to **SI-3** and **SI-9** for more details.

RESULTS AND DISCUSSION

Degradation Kinetics

Hydrolysis was observed for 2-TFMP, 4-TFMP, and 2-Cl-4-TFMP at pH 7 and pH 10 (**Figure 2**), but not for 3-TFMP even at elevated temperatures. In a solution buffered with carbonate to a pH of 10.2, and at a temperature of 40 °C for 24 hours, no degradation of 3-TFMP, nor formation of its hydrolysis TP 3-HBA was observed by HPLC-UV (**Figure S1**). We propose that 3-TFMP is unlikely to undergo hydrolysis in the aqueous environment. It is, however, known to undergo photolysis.[9,22]
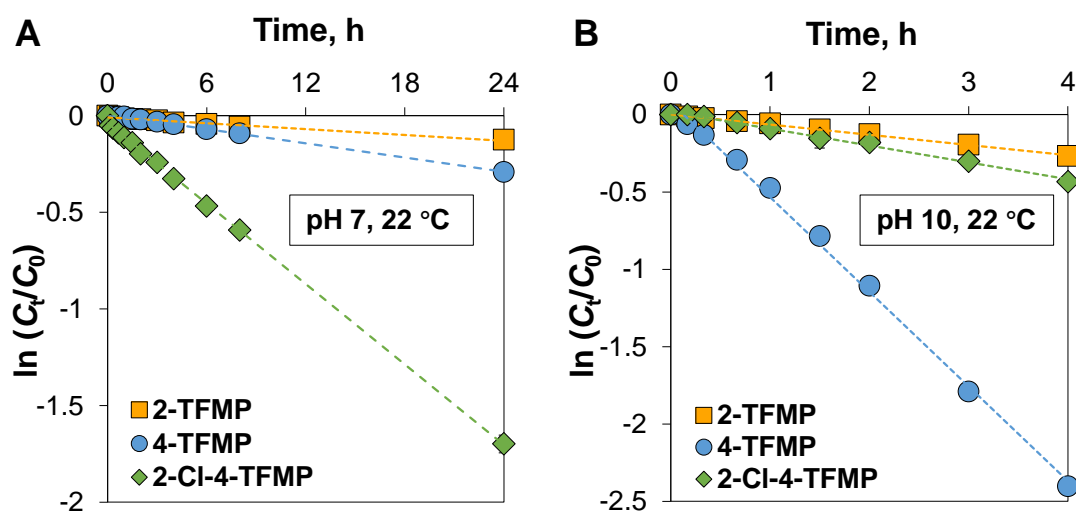
Figure 2. (A) The kinetic plots of 4-TFMP, 2-TFMP and 2-Cl-4-TFMP at a pH of 7.0 ± 0.1 and a temperature of 22 °C ± 1 °C; (B) The kinetic plot of 4-TFMP, 2-TFMP and 2-Cl-4-TFMP at a pH of 10.2 ± 0.1 and a temperature of 22 °C ± 1 °C. Note that the ranges of the x and y-axis in **Figures 2A** and **2B** are different. Results are expressed as mean ± standard deviation; error bars are too small to be seen.
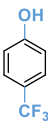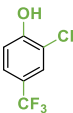
Figure 2A displays the first order kinetics of 2-TFMP, 4-TFMP and 2-Cl-4-TFMP degradation. 2-Cl-4-TFMP reacted at a much faster rate (0.0694 ± 0.0006 h^{-1}) than both 4-

TFMP (0.0147 ± 0.0005 h^{-1}) and 2-TFMP (0.0051 ± 0.0002 h^{-1}). Due to the large difference in

deprotonation between the TFMPs, we propose that the faster reactivity of 2-Cl-4-TFMP is due

to the importance of the role of the deprotonated phenolate species in the hydrolysis reaction.

In a pH 7 solution, 2-Cl-4-TFMP, with a pKa value of 7.09, is 47% deprotonated. Conversely,

4-TFMP has a pKa value of 8.51 and 2-TFMP has a pKa value of 8.12, and thus, at pH 7 are

3.9% and 6.9% deprotonated, respectively (see **Table S3**). The more the TFMP is deprotonated,

the faster it appears to react, suggesting that the pKa of the compound has a considerable impact

on reactivity.

When the compounds were tested in a solution buffered to pH 10.2 ± 0.1, the reactions

rates increased for all TFMPs, and the order of TFMP reaction changed, with 4-TFMP

becoming the fastest. At this pH, over 97% of each TFMP was deprotonated (see **Table S4** for

exact values of deprotonation), so substituent effects could be evaluated. 4-TFMP reacted 41

times faster at pH 10.2 with a rate of 0.612 ± 0.008 h^{-1} compared to its reaction at pH 7 (**Figure**

B and **Table 1**). This is attributed to more 4-TFMP being deprotonated in the alkaline solution.

2-Cl-4-TFMP has a slower reaction rate (0.109 ± 0.004 h^{-1}) than 4-TFMP (**Figure 2**). Similarly

to pH 7, at pH 10 2-TFMP reacted much slower than the other two TFMPs, with a reaction rate

of 0.0661 ± 0.0008 h^{-1}. When tested at an elevated temperature of 30 °C in pH 10 solution, we

were able to compare our 4-TFMP and 2-TFMP degradation rates with those reported by Sakai

and Santi over 50 years ago.[19] We found that our measured rates closely align with theirs (**Table**

1), despite the different buffers used: their experiments in 200 mM borate buffer, and ours in

10 mM carbonate. To the best of our knowledge, there is no previous literature to compare to

our 2-Cl-4-TFMP results.

4-TFMP is the most well-studied TFMP, however, reports on its hydrolytic stability are conflicting. Some suggest 4-TFMP rapidly loses HF upon dissolution in water,[6,20] while others propose that spontaneous defluorination requires conditions that significantly deprotonate the phenol-OH group; otherwise, degradation is minimal, or the hydrolysis defluorination rate is inferred to be extremely slow.[19,21] In ultrapure water (pH_0 5-6), we observed no degradation of 4-TFMP over 4 hours (**Figure S1**), likely due to full protonation of the phenol-OH group. Therefore, we suggest that the spontaneous defluorination of 4-TFMP in aqueous solution is highly reliant on the deprotonation state of its phenol-OH group.

Table 1. Hydrolysis rates and half-lives of TFMPs under various experimental conditions reported here and from the literature. Rates are reported with standard deviations of the mean for results from this work; literature values did not report uncertainties.

Compound	pKa	Buffer/pH/Temperature	Rate (h^{-1})	Half-life (h)
		10 mM phosphate/7/22 °C	0.0147 ± 0.0005	47.0 ± 1.5
		10 mM carbonate/10/22 °C	0.612 ± 0.008	1.13 ± 0.01
	8.51	10 mM carbonate/10/30 °C	1.98 ± 0.03	0.350 ± 0.005
		50 mM borate/8.5/N.A.	[a]0.66	[b]1.1
		200 mM borate/10/30 °C	[c]2.3	[c]0.30
		200 mM phosphate/7/30 °C	[c]0.073	[c]9.5
		10 mM phosphate/7/22 °C	0.0051 ± 0.0002	137 ± 4
		10 mM carbonate/10/22 °C	0.0661 ± 0.0008	10.5 ± 0.1
	8.12	10 mM carbonate/10/30 °C	0.217 ± 0.001	3.19 ± 0.01
		200 mM borate/10/30 °C	[c]0.26	[c]2.7
		200 mM phosphate/7/30 °C	[c]0.0093	[c]74
		10 mM phosphate/7/22 °C	0.0694 ± 0.0006	9.99 ± 0.09
	7.09	10 mM carbonate/10/22 °C	0.109 ± 0.004	6.36 ± 0.24
		10 mM carbonate/10/30 °C	0.431 ± 0.004	1.61 ± 0.01

N.A. = not available; [a] calculated from b; [b] from reference[21]; [c] from reference[19]; values without superscripts are experimental results obtained in this work.
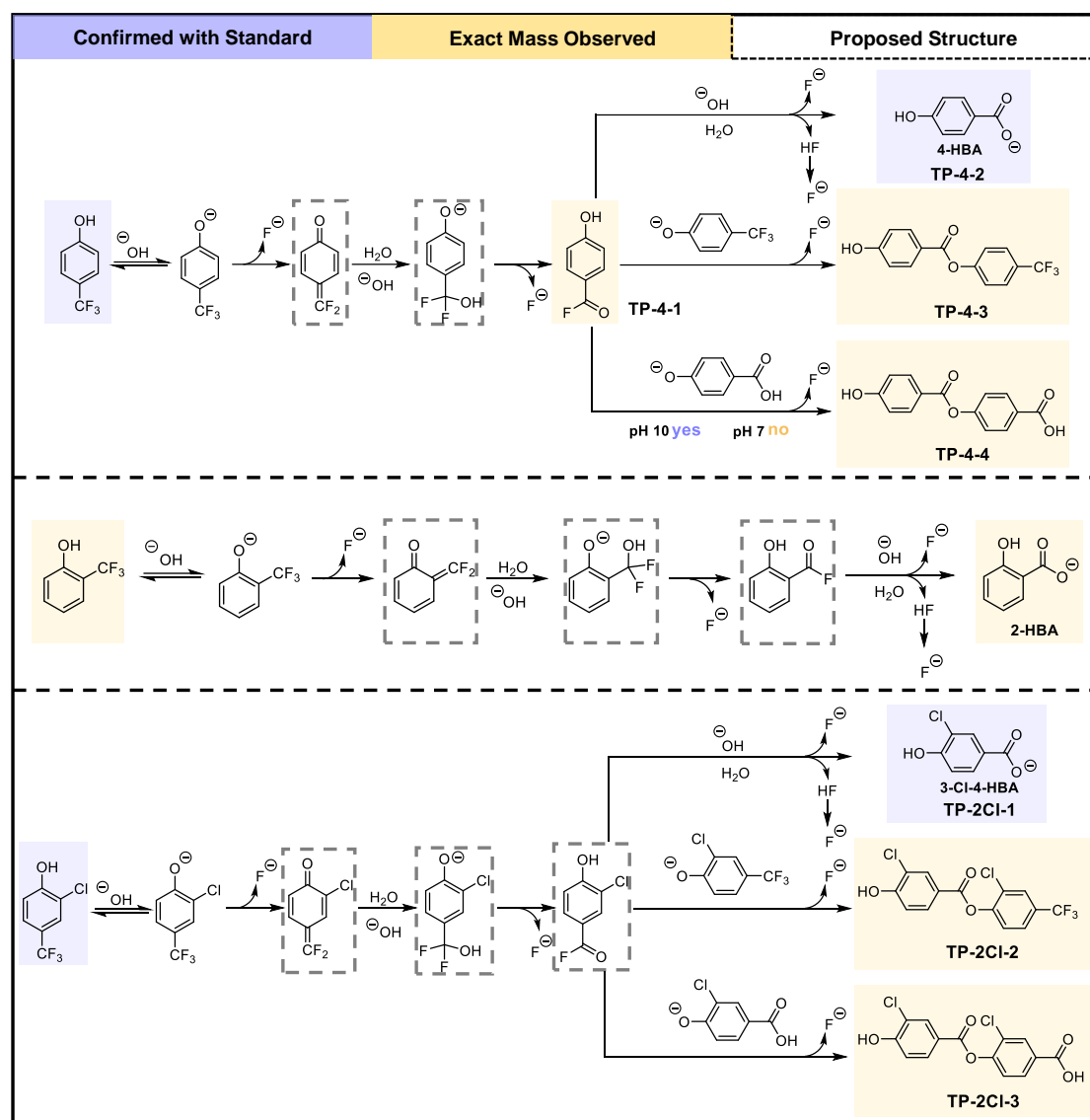
Transformation Products Identification

Hydrolysis of 2-, 4-, and 2-Cl-4-TFMP resulted in the formation of the corresponding HBAs (**Figure S2**). Since the hydrolysis rates of 2-Cl-4- and 2-TFMP at room temperature (22 °C) are much slower than that of 4-TFMP, raising the temperature to 30 °C and 40 °C allowed their reactions to progress sufficiently to compare their HBA formation to that of 4-TFMP. When the reactions neared completion at pH 10 and 40 °C, HBA was formed in near stoichiometric amounts (> 92%) (**Figure S2**). The production of HBA results in the release of three equivalents of F^- as the other product of the reaction. The fluorine mass balance of TFMPs plus F^- (normalized for the 3:1 molar formation ratio) accounted for over 92% of the initial TFMP concentration at each sampling time point (see **Figure S3**). HBA and F^- formation below absolute stoichiometric yields for TFMP hydrolysis can be attributed to the formation of other small amount fluorinated TPs as described below.

HRMS was used to search for additional TPs, either as intermediates of the reaction from TFMPs to HBAs, or other stable products of the reaction. In the hydrolysis of 4-TFMP, the benzoyl fluoride TP-4-1 was observed (**Figure 3**). The formation of this benzoyl fluoride supports the hypothesized pathway where deprotonated 4-TFMP first eliminates F^- and forms a highly reactive conjugated electrophile quinone difluoromethide. This quinone then forms an aryl difluoromethanol ($-CF_2OH$) compound through nucleophilic addition with H_2O or OH^-, and unstable $-CF_2OH$ subsequently eliminates HF to form TP-4-1 (**Figure 3**). Analogous benzoyl fluoride TPs were not observed for other TFMPs, either due to lower formation, or decreased stability of the benzoyl fluorides, resulting in lower concentrations in our samples.

The HRMS of 4-TFMP and 2-Cl-4-TFMP hydrolysis experiments identified novel dimer-

like TPs in addition to HBAs, while for 2-TFMP only 2-HBA was detected (**Figure 3**). TP-4-3,

TP-4-4, TP-2Cl-2 and TP-2Cl-3 are ester TPs whose exact mass was identified (see **Table S6**).

We propose the esterification in TFMP hydrolysis only occurs through the deprotonated

phenolate groups of either TFMP or HBA reacting via a nucleophilic addition-elimination

mechanism with the benzoyl fluoride intermediate. The deprotonation of the phenol-OH is

essential for the ester TP formation. At pH 7, 4-TFMP hydrolysis formed only TP-4-2 and TP-

4-3, with no detection of TP-4-4 after 24 hours. At this pH, the phenol-OH of 4-HBA remains

fully protonated due to its pKa of 9.10 (**Table S5**). At pH 10, the phenol-OH of 4-HBA is 92%

deprotonated. The phenolate (phenol-O$^-$) is a stronger nucleophile than the phenol-OH, and

enables the reaction with benzoyl fluoride to produce TP-4-4. 2-TFMP does not form an ester

analogous to TP-4-4, because the phenol-OH of 2-HBA (salicylic acid) remains fully protonated

at both pH 7 and 10 (see **Table S5**). The lack of the ester analogous to TP-4-3 for 2-TFMP may

be due to the steric hindrance caused by the *ortho*-position of the fluorinated moiety relative to

the phenol-OH. The formation of these esterification products may be limited in the real-world

aqueous environment where concentrations are lower, but it is also possible that other aromatic

pollutants or organic matter with nucleophilic group (–NH$_2$, –OH) in the environment may react

with the benzoyl fluorides.

Figure 3. Proposed reaction mechanism for 4-TFMP, 2-TFMP, and 2-Cl-4-TFMP spontaneous aqueous defluorination.

DFT-Assisted Mechanistic Insights into Spontaneous Defluorination of TFMP

Based on our experimental findings, we determined that the TFMP-phenolate is the species undergoing the hydrolysis reaction and not the protonated TFMP. Thus, we considered scenarios where only the TFMP-phenolate exists. Experimental data at pH 10 was used, and DFT calculations were performed for the TFMP-phenolates only.

Investigation of Rate-Determining Step (RDS)

The initiating step of the spontaneous defluorination of TFMPs involves breaking a strong C–F bond. During this step, the TFMPs undergo dearomatization, leading to an energy increase. We determined that the initiating step is also the rate-determining step (RDS) (**Figure 4C** and **Figure S6**). For the RDS, we examined scenarios starting from the TFMP-phenolate and forming hydrated intermediates with varying numbers of explicit water molecules (**Figure 4A** and **Figure S5**). Discussion on how solvation changes the free energy of activation ($\Delta G^{\ddagger}$, kcal/mol) is given in the Supplementary Information, **SI-9**.

The DFT-calculated $\Delta G^{\ddagger}$ for the hydrolytic defluorination of 4-TFMP (21.2 kcal/mol) and 2-TFMP (22.6 kcal/mol) closely matched the experimental values of 22.6 kcal/mol and 23.5 kcal/mol, respectively (**Table 2**). The calculated $\Delta G^{\ddagger}$ for 2-Cl-4-TFMP falls within the standard deviation range of its experimentally determined $\Delta G^{\ddagger}$. 4-TFMP is the most reactive at pH 10 in our laboratory experiments, and has the lowest $\Delta G^{\ddagger}$ of the three TFMPs determined both experimentally and theoretically. 2-Cl-4-TFMP is more reactive than 2-TFMP (**Figure 2B**), however, based on our $\Delta G^{\ddagger}$ determination, we cannot attribute the faster reactivity to a lower energy RDS. This is because of the larger relative error of our experimental $\Delta G^{\ddagger}$ of 2-Cl-4-TFMP, compared to the other TFMPs. DFT calculations reported the highest $\Delta G^{\ddagger}$ for 2-Cl-4-

277   TFMP, but this does not align with our experimental observations, which suggests the current

278   hybrid solvation model used may be insufficient to fully capture the real conditions. The RDS

279   transition state structures for three TFMPs shared similar key features: stretched C–F bonds,

280   hydrogen-bond interactions between explicit water molecules and the phenolate, and

281   stabilization of the transition state through interactions between the water O-H and the

282   departing F⁻ (**Figure 4A**).
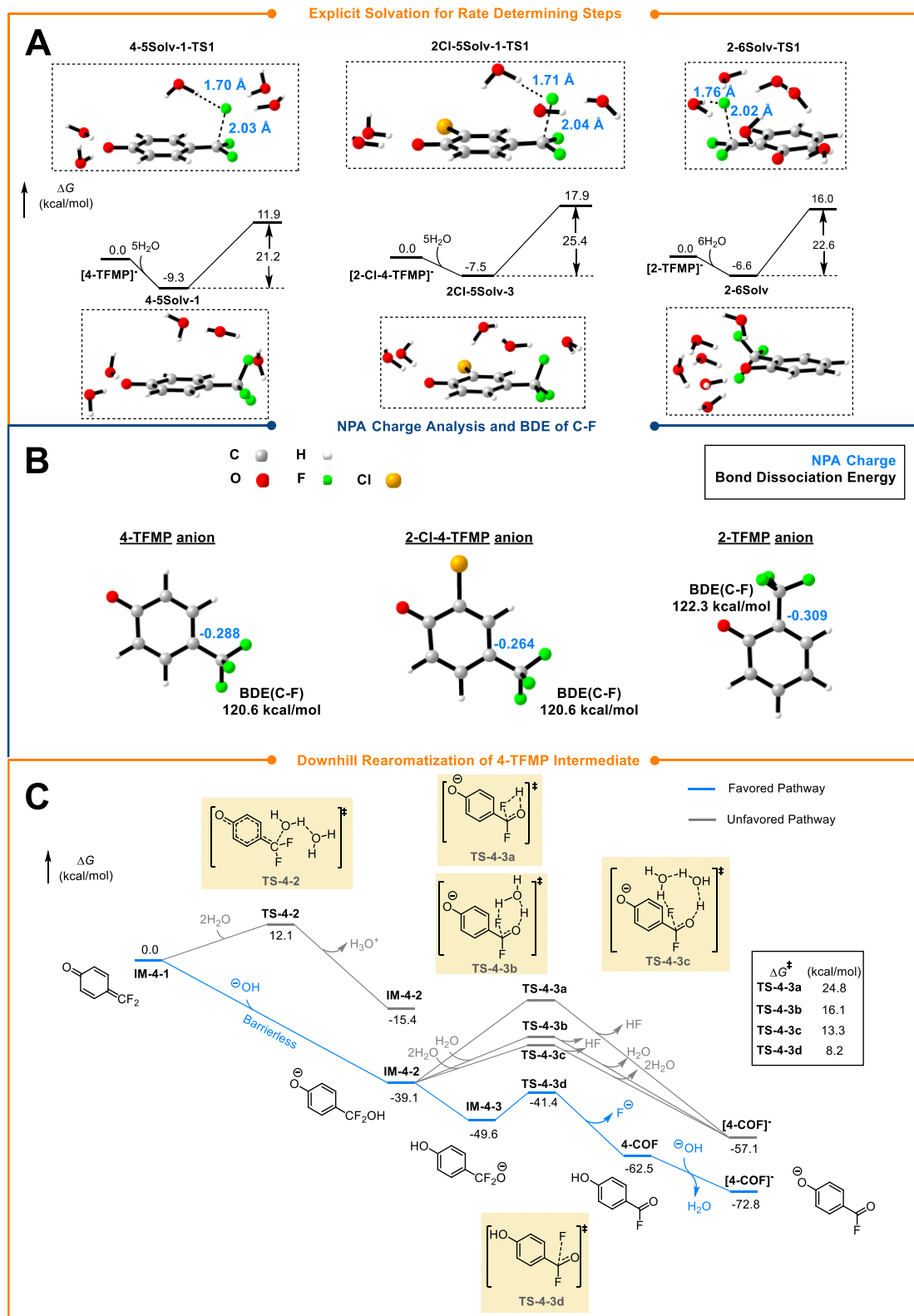
Figure 4. (A) DFT pathways with the minimum energy barriers for 4-, 2-Cl-4-, 2-TFMP aqueous

spontaneous defluorination reactions rate-determining steps under the hybrid solvation model beginning

with the deprotonated TFMP-phenolates; (B) NPA charge of –CF₃'s β-carbons and the bond dissociation

287 energy of C–F bonds in TFMPs (deprotonated, phenolates); CYLview was used to visualize the

288 structures.[35] (C) Downhill rearomatization of quinone difluoromethide intermediate for 4-TFMP.

289

290 **Table 2**. Experimental and DFT-determined free energy of activation ($\Delta G^{\ddagger}$, kcal/mol) of the phenolate

291 species of 2-, 4-, and 2-Cl-4-TFMP spontaneous defluorination. Experimental values of $\Delta G^{\ddagger}$ were

292 calculated from the fitting of **eq 4**. DFT-calculated $\Delta G^{\ddagger}$ were based on hybrid solvation model with

293 different number of explicit water molecules. The RDS pathways with minimum energy barriers for the

294 RDS are shown here, along with the corresponding number of explicit water molecules "$n(H_2O)$"

295 required. A summary of all solvation scenarios for the RDS is provided in the **Table S7**.

TFMP-phenolate	$\Delta G^{\ddagger}_{exp}$	R^2	Minimum $\Delta G^{\ddagger}_{DFT}$ Scenario $n(H_2O)$	$\Delta G^{\ddagger}_{DFT}$
2-TFMP	23.5 ± 1.6	0.995	6	22.6
4-TFMP	22.6 ± 1.8	0.999	5	21.2
2-Cl-4-TFMP	22.8 ± 3.9	0.971	5	25.4

296

Investigation of TFMP-phenolate Electronic Properties

298 The –CF_3 substituents in TFMPs impart environmentally relevant phenol-OH pKa values

299 as a strong electron-withdrawing groups. Then, the deprotonated phenolates promote the

300 cleavage of a C–F bond via a E1cb mechanism, releasing the first F⁻ of *ortho* and *para* –CF_3,

301 giving dearomatized quinone difluoromethides. This process is similar to the environmental

302 transformation of the insecticide DDT into DDE via carbanion-mediated chloride elimination.[36]

303 In contrast, the negative charge does not delocalize to the *meta* position, rendering the *meta* –

304 CF_3 group resistant to β-elimination, as seen with 3-TFMP, which resists hydrolysis even in a

305 pH 10 solution at 40 °C. Additional electron withdrawing groups on the aromatic ring can

306 delocalize the negative charge, thereby decreasing the potential of β-elimination and

defluorination. NPA analysis determined that the β-carbanion in 2-Cl-4-TFMP has a charge of

–0.264, lower (in absolute value) than –0.288 observed in 4-TFMP (**Figure 4B**), aligning well

with lower observed reactivity of 2-Cl-4-TFMP compared to 4-TFMP. Bond dissociation

energy (BDE) calculations further reveal that 4-TFMP and 2-Cl-4-TFMP have equivalent C–F

BDEs (120.6 kcal/mol), whereas 2-TFMP has a higher BDE of 122.3 kcal/mol, corresponding

to its consistently lowest reactivity of the TFMPs studied.

Investigation of the Quinone Difluoromethide Intermediate Rearomatization

After the initiating rate-determining step, the energy profiles of 2-, 4-, and 2-Cl-4-TFMP

are generally downhill, involving barrierless reactions and reactions with low energy barriers

that lead to the rearomatization of the reactive quinone difluoromethide intermediates (**Figure

4C** and **Figure S6**).

In **Figure 4C**, the quinone difluoromethide intermediate IM-4-1 can undergo a barrierless

reaction with OH$^-$ to form the same IM-4-2 (ΔG = –39.1 kcal/mol, see potential energy surface

scan results in **Figure S7**), a rearomatization process that is both thermodynamically and

kinetically favorable. For 2-Cl-4-TFMP and 2-TFMP, the barrierless reaction between OH$^-$ and

their corresponding quinone difluoromethides is also the more favored pathway (illustrated in

Figure S6, with potential energy surface scan results shown in **Figure S7**). These quinone

difluoromethides are highly reactive electrophiles, rapidly captured by OH$^-$ or other

nucleophiles, making them undetectable via regular HRMS or ^{19}F NMR.

For the intermediate IM-4-2, the unstable –CF$_2$OH structure readily eliminates HF via a

hydrogen-bonding network. Adding explicit water molecules to the TS of this HF-elimination

329   reduced $\Delta G^\ddagger$ from 24.8 to 13.3 kcal/mol, consistent with prior studies.[25] Alternatively, IM-4-2

330   can undergo intramolecular proton transfer to form IM-4-3, where the negatively charged

331   oxygen in $-CF_2O^-$ facilitates the leaving of F^- with $\Delta G^\ddagger$ of only 8.2 kcal/mol, making it highly

332   favorable kinetically. Similar scenarios are observed for 2-Cl-4-TFMP and 2-TFMP. After the

333   removal of first two F^-, all three TFMPs generate the corresponding (deprotonated) benzoyl

334   fluorides, which reacts either with H_2O/OH^- to eliminate the last F^- and to form benzoic acids

335   or with other nucleophiles such as phenol-O^- to form dimer-like TPs.

336

337   **Defluorination compared to other PFAS**

338   Despite the extreme environmental persistence of many organofluorine compounds due to

339   the strength of the C–F bond, some compounds undergo partial or complete spontaneous

340   defluorination. In this study, specific TFMPs achieved complete defluorination because, in the

341   RDS, the negative charge of the phenolate is delocalized through conjugation, driving β-

342   elimination of a single F^- to form reactive electrophilic α,β-unsaturated ketones (**Figure 1C**).

343   These α,β-unsaturated ketones immediately undergo further reactions to eliminate the second

344   and the third F^-.

345   Although one carbon involved in the β-elimination defluorination reaction of TFMPs is an

346   aryl-carbon (sp^2 hybridized), and many PFAS molecules are composed of alkyl-carbons (sp^3

347   hybridized), similar β-elimination defluorination mechanisms have been observed in other

348   PFAS chemistry and usually occur in the early stages of the overall reaction. For instance,

349   perfluorooctanoic acid (PFOA) can undergo decarboxylation in polar aprotic solvents, forming

350   a perfluoroalkyl carbanion that drives β-elimination of an adjacent C–F bond to give a

351   perfluoroalkene.[27] DFT calculations revealed a $\Delta G^{\ddagger}$ of 19.5 kcal/mol for this β-elimination

352   step,[27] comparable to the $\Delta G^{\ddagger}$ values observed for TFMPs in our study. For polyfluorinated

353   compounds, it has been reported that the presence of easily removable H or Cl atoms can

354   indirectly trigger defluorination.[37,38] Multiple electron-withdrawing C–F bonds can weaken

355   other chemical bonds to facilitate dissociation. In this work, the phenol-O–H bonds in TFMPs

356   are more readily dissociated than the equivalent non-fluorinated methylphenols (cresols). For

357   example, the pKa of 4-TFMP is 8.51 compared to 10.25 for 4-methylphenol, due to the

358   trifluoromethyl group stabilizing the carbanion. For sp^3-sp^3 hybridized carbons, 6:2, 8:2, 10:2

359   fluorotelomer carboxylic acid (n:2 FTCA, $C_{n-1}F_{2n-1}CF_2CH_2COOH$, n = 6/8/10) can transform

360   into n:2 fluorotelomer unsaturated carboxylic acid (n:2 FTUCA, $C_{n-1}F_{2n-1}CF=CHCOOH$, n =

361   6/8/10) biotically or abiotically.[39,40] This abiotic transformation is facilitated by a base,[39,40]

362   likely through the deprotonation of a C–H adjacent to the carboxyl group, leading to β-

363   elimination and the formation of an α,β-unsaturated carbonyl compound. Similarly, 8:2

364   fluorotelomer aldehyde (8:2 FTAL, $C_7F_{15}CF_2CH_2CHO$) is unstable in water, and loses HF to

365   produce the 8:2 fluorotelomer α,β-unsaturated aldehyde (8:2 FTUAL, $C_7F_{15}CF=CHCHO$).[41] A

366   recent study suggest that an unsaturated perfluorinated compound E-perfluoro-4-methylpent-

367   2-enoic acid [$(CF_3)_2CFCF=CFCOOH$] can undergo microbial defluorination, where similar

368   base-facilitated β-elimination defluorination contributes as part of the mechanism.[37]

369

370   **CONCLUSIONS**

371   Here, we report a comprehensive investigation into the hydrolysis kinetics and

372   defluorination mechanisms of TFMPs in the aqueous phase. Hydrolysis experiments were

373   conducted in pH 7 phosphate buffer and pH 10 carbonate buffer to evaluate the reactivity of 2-,

374   3-, 4-, 2-Cl-4-TFMP. Among these, 2-, 4-, and 2-Cl-4-TFMP showed significant spontaneous

375   defluorination in aqueous solutions, while no hydrolysis of 3-TFMP was observed. The

376   reactivity of TFMPs was strongly influenced by the deprotonation state of the phenol-OH. At

377   pH 7, the TFMPs were only partially deprotonated, resulting in slow reaction kinetics. At pH

378   10, all TFMPs were fully deprotonated, leading to faster reaction kinetics, with relative

379   reactivities following the order 4-TFMP > 2-Cl-4-TFMP > 2-TFMP.

380   HBAs and F^- were the major TPs for the three TFMPs, as confirmed by their molar yields

381   and fluorine mass balance. Orbitrap-HRMS identified new TPs, including a benzoyl fluoride

382   intermediates for 4-TFMP and dimer-like products for 4-TFMP and 2-Cl-4-TFMP, offering

383   additional insights into the reaction mechanisms.

384   The key RDS for defluorination involved β-elimination via an E1cb mechanism, initiated

385   by the deprotonated phenolate. DFT calculations provided detailed insights into this process,

386   highlighting the critical role of water molecule solvation in stabilizing the phenolate and

387   facilitating β-elimination. The reactivity was influenced by both the C–F bond BDE and the

388   negative charge distribution on the phenolate of the TFMPs. Additionally, DFT calculations

389   revealed that following the RDS, the rearomatization of the reactive quinone difluoromethide

390   intermediate was highly favorable both thermodynamically and kinetically. These findings

391   enhance our understanding of defluorination pathways for TFMPs and provide insights into the

392   defluorination chemistry of other PFAS. This may be used to design aryl-CF_3 compounds that

393   favour defluorination in the environment, thus minimizing their environmental impact.

394

Supporting information

The Supporting Information, including DFT results, is available free of charge **online**. References in the **SI** that are not in the main text are cited here.[42–52]

REFERENCES

1 Y. Ogawa, E. Tokunaga, O. Kobayashi, K. Hirai and N. Shibata, Current Contributions of Organofluorine Compounds to the Agrochemical Industry, *iScience*, 2020, **23**, 101467.

2 M. Inoue, Y. Sumii and N. Shibata, Contribution of Organofluorine Compounds to Pharmaceuticals, *ACS Omega*, 2020, **5**, 10633–10640.

3 N. A. Meanwell, Fluorine and Fluorinated Motifs in the Design and Application of Bioisosteres for Drug Design, *J. Med. Chem.*, 2018, **61**, 5822–5880.

417   4 M. Patel, R. Kumar, K. Kishor, T. Mlsna, C. U. Jr. Pittman and D. Mohan, Pharmaceuticals

418   of Emerging Concern in Aquatic Systems: Chemistry, Occurrence, Effects, and Removal

419   Methods, *Chem. Rev.*, 2019, **119**, 3510–3673.

420   5 N. Donley, C. Cox, K. Bennett, A. M. Temkin, D. Q. Andrews and O. V. Naidenko, Forever

421   Pesticides: A Growing Source of PFAS Contamination in the Environment, *Environ. Health*

422   *Perspect.*, 2024, **132**, 075003.

423   6 M. W. Lam, C. J. Young and S. A. Mabury, Aqueous Photochemical Reaction Kinetics and

424   Transformations of Fluoxetine, *Environ. Sci. Technol.*, 2005, **39**, 513–522.

425   7 S. Tisler, F. Zindler, F. Freeling, K. Nödler, L. Toelgyesi, T. Braunbeck and C. Zwiener,

426   Transformation Products of Fluoxetine Formed by Photodegradation in Water and

427   Biodegradation in Zebrafish Embryos (Danio rerio), *Environ. Sci. Technol.*, 2019, **53**, 7400–

428   7409.

429   8 A. C. Altamura, A. R. Moro and M. Percudani, Clinical Pharmacokinetics of Fluoxetine, *Clin.*

430   *Pharmacokinet.*, 1994, **26**, 201–214.

431   9 A. P. Bhat, T. F. Mundhenke, Q. T. Whiting, A. A. Peterson, W. C. K. Pomerantz and W. A.

432   Arnold, Tracking Fluorine during Aqueous Photolysis and Advanced UV Treatment of

433   Fluorinated Phenols and Pharmaceuticals Using a Combined 19F-NMR, Chromatography,

434   and Mass Spectrometry Approach, *ACS Environ. Au*, 2022, **2**, 242–252.

435   10   Z. Guo, A. Attar, Q. Qiqige, R. Lundgren and S. Joudan. Mechanistic Insights into a

436   Fluoxetine-Related Aryl-CF3 Compound. *Revisions Requested at Environmental Science &*

437   *Technology*. Available to read on ChemRxix: https://doi.org/10.26434/chemrxiv-2024-9ql22

438   11   D. Vialaton, D. Baglio, A. Paya-Perez and C. Richard, Photochemical transformation of

439 acifluorfen under laboratory and natural conditions, *Pest Manag. Sci.*, 2001, **57**, 372–379.

440 12 L. Chen, T. Cai and Q. Wang, Characterization of Fluoroglycofen Ethyl Degradation by

441 Strain Mycobacterium phocaicum MBWY-1, *Curr. Microbiol.*, 2011, **62**, 1710–1717.

442 13 S. K. Chakraborty, A. Bhattacharyya and A. Chowdhury, Degradation of Oxyfluorfen by

443 Azotobacter chroococcum (Beijerink), *Bull. Environ. Contam. Toxicol.*, 2002, **69**, 203–209.

444 14 J. Quintana, A. Hernández, F. Ventura, R. Devesa and M. R. Boleda, Identification of 3-

445 (trifluoromethyl)phenol as the malodorous compound in a pollution incident in the water

446 supply in Catalonia (N.E. Spain), *Environ. Sci. Pollut. Res.*, 2019, **26**, 16076–16084.

447 15 T. Chonova, S. Ruppe, I. Langlois, D. S. Griesshaber, M. Loos, M. Honti, K. Fenner and

448 H. Singer, Unveiling industrial emissions in a large European river: Insights from data mining

449 of high-frequency measurements, *Water Res.*, 2025, **268**, 122745.

450 16 Z. Wang, A. M. Buser, I. T. Cousins, S. Demattio, W. Drost, O. Johansson, K. Ohno, G.

451 Patlewicz, A. M. Richard, G. W. Walker, G. S. White and E. Leinala, A New OECD Definition

452 for Per- and Polyfluoroalkyl Substances, *Environ. Sci. Technol.*, 2021, **55**, 15575–15578.

453 17 OECD, *Reconciling Terminology of the Universe of Per- and Polyfluoroalkyl Substances:*

454 *Recommendations and Practical Guidance*, Organisation for Economic Co-operation and

455 Development, Paris, 2021.

456 18 R. G. Jones, Ortho and Para Substituted Derivatives of Benzotrifluoride, *J. Am. Chem. Soc.*,

457 1947, **69**, 2346–2350.

458 19 T. T. Sakai and D. V. Santi, Hydrolysis of hydroxybenzotrifluorides and fluorinated uracil

459 derivatives. General mechanism for carbon-fluorine bond labilization, *J. Med. Chem.*, 1973,

460 **16**, 1079–1084.

461   20   D. A. Ellis and S. A. Mabury, The Aqueous Photolysis of TFM and Related

462   Trifluoromethylphenols. An Alternate Source of Trifluoroacetic Acid in the Environment,

463   *Environ. Sci. Technol.*, 2000, **34**, 632–637.

464   21   D. A. Jackson and S. A. Mabury, Environmental properties of pentafluorosulfanyl

465   compounds: Physical properties and photodegradation, *Environ. Toxicol. Chem.*, 2009, **28**,

466   1866–1873.

467   22   A. Manfrin, A. Hänggli, J. van den Wildenberg and K. McNeill, Substituent Effects on the

468   Direct Photolysis of Benzotrifluoride Derivatives, *Environ. Sci. Technol.*, 2020, **54**, 11109–

469   11117.

470   23   D. C. Thompson, K. Perera and R. London, Spontaneous hydrolysis of 4-

471   trifluoromethylphenol to a quinone methide and subsequent protein alkylation, *Chem. Biol.*

472   *Interact.*, 2000, **126**, 1–14.

473   24   H. Amii and K. Uneyama, C−F Bond Activation in Organic Synthesis, *Chem. Rev.*, 2009,

474   **109**, 2119–2183.

475   25   Y. Zhang, A. Moores, J. Liu and S. Ghoshal, New Insights into the Degradation Mechanism

476   of Perfluorooctanoic Acid by Persulfate from Density Functional Theory and Experimental

477   Data, *Environ. Sci. Technol.*, 2019, **53**, 8672–8681.

478   26   Y. Zhang, J. Liu, S. Ghoshal and A. Moores, Density Functional Theory Calculations

479   Decipher Complex Reaction Pathways of 6:2 Fluorotelomer Sulfonate to Perfluoroalkyl

480   Carboxylates Initiated by Hydroxyl Radical, *Environ. Sci. Technol.*, 2021, **55**, 16655–16664.

481   27   B. Trang, Y. Li, X.-S. Xue, M. Ateia, K. N. Houk and W. R. Dichtel, Low-temperature

482   mineralization of perfluorocarboxylic acids, *Science*, 2022, **377**, 839–845.

483   28   Z. Chen, J. Chen, S. Tan, Z. Yang and Y. Zhang, Dechlorination Helps Defluorination:

484   Insights into the Defluorination Mechanism of Florfenicol by S-nZVI and DFT Calculations

485   on the Reaction Pathways, *Environ. Sci. Technol.*, 2024, **58**, 2542–2553.

486   29   M. J. Frisch, G. W. Trucks, H. B. Schlegel, G. E. Scuseria, M. A. Robb, J. R. Cheeseman,

487   G. Scalmani, V. Barone, G. A. Petersson, H. Nakatsuji, X. Li, M. Caricato, A. V. Marenich, J.

488   Bloino, B. G. Janesko, R. Gomperts, B. Mennucci, H. P. Hratchian, J. V. Ortiz, A. F. Izmaylov,

489   J. L. Sonnenberg, Williams, F. Ding, F. Lipparini, F. Egidi, J. Goings, B. Peng, A. Petrone, T.

490   Henderson, D. Ranasinghe, V. G. Zakrzewski, J. Gao, N. Rega, G. Zheng, W. Liang, M. Hada,

491   M. Ehara, K. Toyota, R. Fukuda, J. Hasegawa, M. Ishida, T. Nakajima, Y. Honda, O. Kitao,

492   H. Nakai, T. Vreven, K. Throssell, J. A. Montgomery Jr., J. E. Peralta, F. Ogliaro, M. J.

493   Bearpark, J. J. Heyd, E. N. Brothers, K. N. Kudin, V. N. Staroverov, T. A. Keith, R. Kobayashi,

494   J. Normand, K. Raghavachari, A. P. Rendell, J. C. Burant, S. S. Iyengar, J. Tomasi, M. Cossi,

495   J. M. Millam, M. Klene, C. Adamo, R. Cammi, J. W. Ochterski, R. L. Martin, K. Morokuma,

496   O. Farkas, J. B. Foresman and D. J. Fox, Gaussian 16 Rev. C.01, Gaussian, Inc., Wallingford,

497   CT, USA, 2016.

498   30   E. Cancès, B. Mennucci and J. Tomasi, A new integral equation formalism for the

499   polarizable continuum model: Theoretical background and applications to isotropic and

500   anisotropic dielectrics, *J. Chem. Phys.*, 1997, **107**, 3032–3041.

501   31   N. Mardirossian and M. Head-Gordon, How Accurate Are the Minnesota Density

502   Functionals for Noncovalent Interactions, Isomerization Energies, Thermochemistry, and

503   Barrier Heights Involving Molecules Composed of Main-Group Elements?, *J. Chem. Theory

504   Comput.*, 2016, **12**, 4303–4325.

32   Y. Zhao and D. G. Truhlar, The M06 suite of density functionals for main group thermochemistry, thermochemical kinetics, noncovalent interactions, excited states, and transition elements: two new functionals and systematic testing of four M06-class functionals and 12 other functionals, *Theor. Chem. Acc.*, 2008, **120**, 215–241.

33   A. V. Marenich, C. J. Cramer and D. G. Truhlar, Universal Solvation Model Based on Solute Electron Density and on a Continuum Model of the Solvent Defined by the Bulk Dielectric Constant and Atomic Surface Tensions, *J. Phys. Chem. B*, 2009, **113**, 6378–6396.

34   W. Qin, K. Guo, C. Chen and J. Fang, Differences in the Reaction Mechanisms of Chlorine Atom and Hydroxyl Radical with Organic Compounds: From Thermodynamics to Kinetics, *Environ. Sci. Technol.*, 2024, **58**, 17886–17897.

35   C. Y. Legault, CYLview20, Université de Sherbrooke, 2020 (http://www.cylview.org).

36   R. P. Schwarzenbach, P. M. Gschwend and D. M. Imboden, Environmental organic chemistry, Wiley, Third edition., 2017.

37   Y. Yu, F. Xu, W. Zhao, C. Thoma, S. Che, J. E. Richman, B. Jin, Y. Zhu, Y. Xing, L. Wackett and Y. Men, Electron bifurcation and fluoride efflux systems implicated in defluorination of perfluorinated unsaturated carboxylic acids by Acetobacterium spp, *Sci. Adv.*, 2024, **10**, eado2957.

38   S. Che, B. Jin, Z. Liu, Y. Yu, J. Liu and Y. Men, Structure-Specific Aerobic Defluorination of Short-Chain Fluorinated Carboxylic Acids by Activated Sludge Communities, *Environ. Sci. Technol. Lett.*, 2021, **8**, 668–674.

39   J. Liu and S. Mejia Avendaño, Microbial degradation of polyfluoroalkyl chemicals in the environment: A review, *Environ. Int.*, 2013, **61**, 98–114.

527   40   M. Loewen, T. Halldorson, F. Wang and G. Tomy, Fluorotelomer Carboxylic Acids and

528   PFOS in Rainwater from an Urban Center in Canada, *Environ. Sci. Technol.*, 2005, **39**, 2944–

529   2951.

530   41   J. W. Martin, S. A. Mabury and P. J. O'Brien, Metabolic products and pathways of

531   fluorotelomer alcohols in isolated rat hepatocytes, *Chem. Biol. Interact.*, 2005, **155**, 165–180.

532   42   J. J. Fifen, Z. Dhaouadi and M. Nsangou, Revision of the Thermodynamics of the Proton

533   in Gas Phase, *J. Phys. Chem. A*, 2014, **118**, 11090–11097.

534   43   J. R. P. Jr and J. M. Riveros, Gibbs energy of solvation of organic ions in aqueous and

535   dimethyl sulfoxide solutions, *Phys. Chem. Chem. Phys.*, 2002, **4**, 1622–1627.

536   44   M. D. Tissandier, K. A. Cowen, W. Y. Feng, E. Gundlach, M. H. Cohen, A. D. Earhart, J.

537   V. Coe and T. R. Tuttle, The Proton's Absolute Aqueous Enthalpy and Gibbs Free Energy of

538   Solvation from Cluster-Ion Solvation Data, *J. Phys. Chem. A*, 1998, **102**, 7787–7794.

539   45   A. E. Reed, R. B. Weinstock and F. Weinhold, Natural population analysis, *J. Chem. Phys.*,

540   1985, **83**, 735–746.

541   46   S. P. Ozkorucuklu, J. L. Beltrán, G. Fonrodona, D. Barrón, G. Alsancak and J. Barbosa,

542   Determination of Dissociation Constants of Some Hydroxylated Benzoic and Cinnamic Acids

543   in Water from Mobility and Spectroscopic Data Obtained by CE-DAD, *J. Chem. Eng. Data*,

544   2009, **54**, 807–811.

545   47   *CRC handbook of chemistry and physics : a ready-reference book of chemical and physical

546   data*, CRC Press, Taylor & Francis Group, 2018th–2019th, 99th edition edn., 2018.

547   48   A. Arcelli and C. Concilio, Polyelectrolyte effects exerted by poly(ethyleneimine) on the

548   ionization constant of substituted phenols, *J. Chem. Soc. Perkin Trans. 2*, 1989, 887–892.

549 49 L. Martínez, R. Andrade, E. G. Birgin and J. M. Martínez, PACKMOL: A package for

550   building initial configurations for molecular dynamics simulations, *J. Comput. Chem.*, 2009,

551   **30**, 2157–2164.

552 50 A. K. Rappe, C. J. Casewit, K. S. Colwell, W. A. I. Goddard and W. M. Skiff, UFF, a full

553   periodic table force field for molecular mechanics and molecular dynamics simulations, *J.*

554   *Am. Chem. Soc.*, 1992, **114**, 10024–10035.

555 51 C. Bannwarth, S. Ehlert and S. Grimme, GFN2-xTB—An Accurate and Broadly

556   Parametrized Self-Consistent Tight-Binding Quantum Chemical Method with Multipole

557   Electrostatics and Density-Dependent Dispersion Contributions, *J. Chem. Theory Comput.*,

558   2019, **15**, 1652–1671.

559 52 C. Bannwarth, E. Caldeweyher, S. Ehlert, A. Hansen, P. Pracht, J. Seibert, S. Spicher and

560   S. Grimme, Extended tight-binding quantum chemistry methods, *WIREs Comput. Mol. Sci.*,

561   2021, **11**, e1493.

562